Reduction of secondary-electron yields by collective electric fields within metals

Joseph E. Borovsky and David M. Suszcynsky
Space Plasma Physics Group, Los Alamos National Laboratory, Los Alamos, New Mexico 87545
(Received 29 May 1990)

A fast ion passing through a metal target drives electrons out of its path by means of Coulomb scattering. Some of these electrons escape the target and are denoted as secondary electrons. The rapid displacement of electrons from the ion's path produces a charge separation in the metal, which gives rise to an electric field in the wake of the ion. For $z > 1$ ions, the wake fields can be so strong that they retard the movement of electrons away from the ion's path, which reduces the number of secondary electrons that escape the target. The time-dependent electric fields behind fast ions in metals are modeled and the motion of Coulomb-scattered electrons in these fields is examined. The fraction of the electrons that are trapped by the wake is estimated and from this the reduction in the yield of secondary electrons is quantified. The results are in agreement with measurements of secondary-electron emission by fast, high-z ions hitting metal targets.

I. INTRODUCTION

When a high-velocity ion (where E is greater than or equal to a few MeV/amu) passes into a solid target, electrons are knocked out of the target. These knocked-out electrons are denoted as secondary electrons. Three basic processes occur in the ejection of electrons: (i) electrons in the target are energized by means of Coulomb scattering, (ii) the electrons are transported to the target surface, and (iii) electrons cross the surface into vacuum.

There are two types of theoretical models for the emission of secondary electrons when a fast projectile encounters a target: single-particle models and cascade models. In the single-particle models[1,2] each electron that escapes from the target is assumed to have been directly ionized from the target lattice by the fast ion. In the cascade models[3–5] some of the electrons that escape from the target are assumed to have been ionized from the target lattice by secondary and tertiary collisions with other electrons. Both models treat the transport of electrons away from the ion's path without accounting for the collective electric fields that arise from the removal of negative charge from the vicinity of the ion's path. Both types of models predict that the yield of secondary electrons Y (Y is the number of electrons ejected from the target per incident ion) is linearly proportional to the electronic stopping power dE/dx of the target material to the fast ion;[6] i.e., more energy deposited produces more secondaries. In the model of Sternglass,[1] the secondary-electron yield is given by

$$Y_0 = \frac{Pd_s}{E_*}\frac{dE}{dx} , \tag{1}$$

where d_s is the mean depth from which secondary electrons originate, E_* is the average amount of kinetic energy deposited by the ion into the target per ionization produced in the target, and $P \approx \frac{1}{2}$ is the probability for an ionization electron to have a net motion toward the surface of the target. A subscript "0" is added to Y to denote an uncorrected value. The work function of the surface can be accounted for in P. In the theoretical models, the combination Pd_s/E_* is a constant for each type of target: Pd_s/E_* is independent of the type of incident ion and of the ion velocity. Typically Pd_s/E_* is of the order 1 Å/eV. If cascade processes are occurring, Eq. (1) basically still holds, but the physical interpretation of P and E_* may change.

When the secondary-electron yield is high, this picture of secondary-electron emission needs to be modified. There is evidence for this in the secondary-electron-emission measurements of Refs. 7 and 8, where the measured yields are less than the predicted yields. The needed modification to the picture is the following. When a fast ion travels through the target, it transfers kinetic energy to electrons along its path by means of Coulomb scattering. These electrons move outwards in a swarm away from the ion's path leaving a region of positive charge in the wake of the ion (see Fig. 1). Within the metal target, the electric field of this space-charge separation acts to retard the outward motion of the electrons. If the number of outward-moving electrons is large enough, then the electric fields will be strong enough to recapture electrons in the swarm and these electrons will no longer contribute to the secondary-electron yield. Hence the collective electric fields lessen the yield and therefore need to be accounted for in the theoretical models. This modeling will be somewhat complicated because conduction-band electrons in the metal will respond and shield out the space-charge separation on a time scale comparable to the time scale for the electron swarm to move away from the ion's path.

The role of the wake electric field in recapturing electrons within the target was suggested in Ref. 8. It differs from the role that Koyama *et al.*[7] suggested, which was the recapturing of the secondary electrons by the electric field outside of the metal target, a process that would have to occur long after plasmon shielding acted on the electric fields. The wake considered here is caused by the displacement of electrons from the path of an ion by

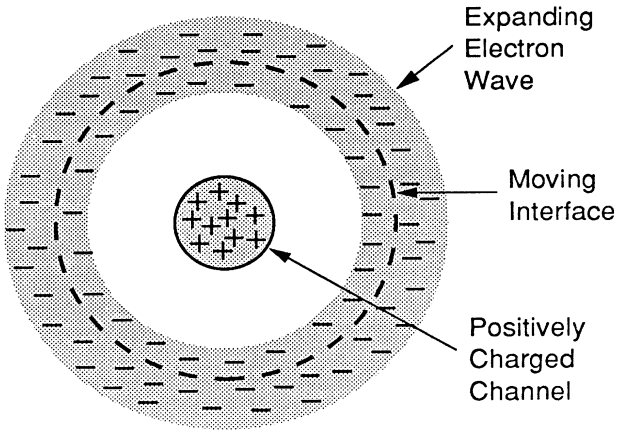

FIG. 1. Cross section of the path of the ion showing the outward-moving swarm of electrons and the positive charge left behind.

two-body scattering. A more commonly studied wake is the fluid reaction of the conduction-band electron gas to the moving charge of the ion, which leads to the Cerenkov emission of plasmons. Typically, the plasmon wake is studied by a linear dielectric response to the moving charge,[9–12] as is done for the Langmuir-wave wake in Maxwellian plasmas[9,13] and the density-wave wake in Maxwellian gases of stars.[14,15] In plasmas, computer-simulation techniques are now being used to determine the nonlinear wake of plasma waves for fast-moving charges.[16–18] The need for a nonlinear treatment of the conduction-band wake has been pointed out in Ref. 19. The wake caused by the two-body scattering of electrons out of the path of an ion has been treated[20–22] by adding a term in the dielectric response function that has a group velocity equal to the speed of an electron receiving a Coulomb kick with impact parameter $b=2\pi/k$, with k being the wave number. This simulates a burst of electrons moving out from the path of the ion. However, this treatment requires the wake to be of small amplitude. The dual wake (fluid reaction giving plasmons and two-body reactions giving electron bursts) launched by the moving ion is similar to the dual launching of plasma waves (fluid reactions) and pseudowaves (particle bursts) from a charged object in a Maxwellian plasma.[23,24] One other type of wake considered for fast particles moving through targets arises from the polarization of atomic orbitals owing to the electric field of the moving particle.[25,26]

In this paper the effects of the dual wake (two-body electron motion plus fluid electron motion) on the transport of electrons in metal targets and on the production of secondary electrons will be estimated. First the time-dependent charge separation in the ion wake is estimated from Coulomb-scattering statistics and electron binding-energy arguments. Then Gauss's law is solved to get the electric field produced by the charge separation. The motion of Coulomb-scattered electrons in the collective electric field is determined by computationally solving the equation of motion and analytically fitting the solution. The plasma-frequency response of conduction-band electrons to the charge separation is accounted for and the collective electric field is switched off after a fraction of a plasma period. In this manner, the fraction of the Coulomb-scattered electrons that are electrostatically trapped in the ion wake is determined and the reduction of the secondary-electron yield owed to this trapping is calculated.

II. THE METHOD USED TO DETERMINE THE REDUCED YIELD

As a fast ion travels within a metal target, conduction-band electrons and valence electrons of the metal are energized by means of Coulomb scattering. The velocity vectors of the electrons after the Coulomb scattering are oriented at approximately 90° to the ion's path, so the passage of the ion produces a swarm of electrons moving radially outward from the path. For a collision with impact parameter b, an electron will obtain an energy kick ΔE given by[27]

$$\Delta E=2\frac{z^2e^4}{m_ev_0^2}\frac{1}{b^2+z^2e^4/m_e^2v_0^4}\ , \tag{2}$$

where v_0 is the velocity of the fast ion and z is the charge state of the ion. For a uniform density of electrons in the metal, the distribution of impact parameters b between the ion's path and the electrons of the metal is $f(b)db=2\pi bdb$ (see Ref. 27). Requiring $f(\Delta E)d\Delta E=f(b)db$ and obtaining $db/d\Delta E$ from Eq. (2), the distribution of energy kicks is found to be

$$f(\Delta E)=-\frac{4\pi}{\Delta E^2}\frac{z^2e^4}{m_ev_0^2}\ . \tag{3}$$

The number of electrons receiving energy kicks from the ion is proportional to $\int_0^{b_{\max}}f(b)db$, where $b_{\max}$ is a cutoff impact parameter that will be set by a minimum ΔE value in Eq. (2). This can be written as $\int_0^{b_{\max}}f(b)db=-\int_{\Delta E_{\min}}^{\Delta E_{\max}}f(\Delta E)d\Delta E$. The maximum energy kick $\Delta E_{\max}$ occurs for $b=0$; Eq. (2) yields $\Delta E_{\max}=2m_ev_0^2$. The minimum energy kick $\Delta E_{\min}$ is related to the ionization energy of the metal atoms: if ΔE is below the ionization energy of the electron, then the electron will not be freed by the ion so that the energy kick is not counted. As an average to the lower limit of integration $\Delta E_{\min}$, the mean ionization energy I of the metal atoms is taken, so $\Delta E_{\min}=I$. If collective electric-field effects are ignored, then, whether or not cascade processes are important, the yield of secondary electrons (Y is the number of electrons escaping the metal per ion impact) will be linearly proportional to the number of electrons freed $-\int_{\Delta E_{\min}}^{\Delta E_{\max}}f(\Delta E)d\Delta E$, with a constant of proportionality that depends on electron-transport processes, cascade efficiencies, etc. Using the above values for $\Delta E_{\max}$ and $\Delta E_{\min}$, the secondary-electron yield takes the form

$$Y_0=C\int_I^{2m_ev_0^2}\frac{1}{\Delta E^2}d\Delta E\ , \tag{4}$$

where the subscript 0 indicates that the collective electric-field effects are not accounted for and where C is a constant. Performing the integration results in

$$Y_0 = C\left[\frac{1}{I} - \frac{1}{2m_e v_0^2}\right] . \tag{5}$$

According to the secondary-electron-emission model of Sternglass,[1] the secondary-electron yield is given by Eq. (1). Combining relations (5) and (1) obtains the constant C:

$$C = \frac{Pd_s}{E_*}\frac{dE}{dx}\left[\frac{1}{I} - \frac{1}{2m_e v_0^2}\right]^{-1} . \tag{6}$$

The effect of the collective electric field of the space-charge separation is to raise the lower limit of integration on the distribution $f(\Delta E)$ in Eq. (4). Because the electrons must climb out of the potential well to escape, an electron needs $\Delta E_{\min} + e\Delta\phi_{\text{trap}}$ of energy to escape rather than $\Delta E_{\min}$ of energy, where $\Delta\phi_{\text{trap}}$ is the depth of the potential well that traps electrons (which is estimated below). Making the replacement of the lower limit of integration in expression (4), using expression (6) for C, and using $\Delta E_{\max} = 2m_e v_0^2$ and $\Delta E_{\min} = I$ obtains an expression for the true number of secondaries

$$Y_{\text{true}} = \frac{Pd_s}{E_*}\frac{dE}{dx}\left[\frac{1}{I} - \frac{1}{2m_e v_0^2}\right]^{-1} \times \left[\frac{1}{I + e\Delta\phi_{\text{trap}}} + \frac{1}{2m_e v_0^2}\right] . \tag{7}$$

Note that the trapping potential $\Delta\phi_{\text{trap}}$ will be a function of the yield Y_{true}.

As the distribution of Coulomb-scattered electrons moves radially outward from the path of the ion, velocity dispersion will spread out the electron swarm, with the faster electrons obtaining greater r values than the slower electrons. Inside this electron swarm there will be an outward-moving interface that separates electrons with sufficient kinetic energy to escape the ion's wake from electrons without sufficient kinetic energy (see Fig. 1). This interface travels with the velocity of an electron that is turned around by the charge-separation electric field at the instant that the charge-separation field is turned off. Electrons faster than this interface escape to produce secondary electrons and electrons slower than this interface are trapped in the wake. Gauss's law $\nabla\cdot\mathcal{E} = 4\pi n_q$ for a cylindrically symmetric charge distribution n_q yields the electric field

$$\mathcal{E} = \frac{2}{r}\left[\frac{Q}{L}\right]_{\text{interior}} , \tag{8}$$

where $(Q/L)_{\text{interior}}$ is the charge per unit length interior to radius r. The charge distribution near the ion's path is depicted in Fig. 1. Behind the ion there will be a positively charged channel with a radius r_{ch} from which electrons have been expelled by Coulomb scattering. If cascade processes are not occurring, then the charge per unit length of the positive channel is $Q/L = eY_{\text{true}}/Pd_s$, since Y_{true}/P electrons are removed from a length of ion path d_s long to produce the secondary-electron yield Y_{true}. This is generalized to include cascade processes by defining F_{casc} to be the fraction of the secondary electrons that are directly produced by Coulomb scattering and not by cascade processes. Then $1/F_{\text{casc}}$ is the multiplicative factor for Coulomb-scattered electrons to drive a cascade of free electrons. With cascade processes operating, the charge per unit length of the positive channel is $Q/L = eF_{\text{casc}}Y_{\text{true}}/Pd_s$. For simplicity the charge density in the cylindrical channel is taken to be uniform; hence

$$n_q = (eF_{\text{casc}}Y_{\text{true}}/Pd_s)/\pi r_{\text{ch}}^2 , \tag{9}$$

where r_{ch} is the channel radius, which is expressed in terms of a typical impact parameter for electron displacement. Setting $b = r_{\text{ch}}$ in expression (2), the channel radius is expressed as

$$r_{\text{ch}}^2 = \frac{2z^2e^4}{m_e v_0^2}\left[\frac{1}{\Delta E_{\text{ch}}} + \frac{1}{2m_e v_0^2}\right] , \tag{10}$$

where ΔE_{ch} is an energy kick that defines the channel width. Outside of the channel, the positive charge density is zero. Whether or not the trapped electrons are outside of the channel, their charge density interior to the interface is accounted for since $F_{\text{casc}}Y_{\text{true}}$ rather than $F_{\text{casc}}Y_0$ was used for the positive charge density of the channel. The charge density per unit length interior to the interface when the interface is at r is $\int_0^r n_q 2\pi r\, dr$, which gives

$$\left[\frac{Q}{L}\right]_{\text{interior}} = \begin{cases} \dfrac{eF_{\text{casc}}Y_{\text{true}}}{Pd_s}\left[\dfrac{r}{r_{\text{ch}}}\right]^2 & \text{for } r \le r_{\text{ch}} \quad (11a) \\ \dfrac{eF_{\text{casc}}Y_{\text{true}}}{Pd_s} & \text{for } r \ge r_{\text{ch}} . \quad (11b) \end{cases}$$

Using this in expression (8), the collective electric field is

$$\mathcal{E} = \begin{cases} 2\dfrac{eF_{\text{casc}}Y_{\text{true}}}{Pd_s}\dfrac{r}{r_{\text{ch}}^2} & \text{for } r \le r_{\text{ch}} \quad (12a) \\ 2\dfrac{eF_{\text{casc}}Y_{\text{true}}}{Pd_s}\dfrac{1}{r} & \text{for } r \ge r_{\text{ch}} . \quad (12b) \end{cases}$$

The total potential drop $\Delta\phi_{\text{trap}}$ that an electron traveling with the interface experiences is obtained by integrating the electric field of expression (12) from $r = 0$ to $r_{\max}$, where $r_{\max}$ is the position of the interface when the electric field is switched off. The value of $r_{\max}$ will be obtained by computationally solving the equations of motion for an electron moving with the interface.

The position of the interface is obtained by solving

$$\frac{\partial^2 r}{\partial t^2} = -\frac{e}{m_e}\mathcal{E} \tag{13}$$

for the electric fields of Eqs. (12). An analytic solution of this would require dealing with probability integrals. Instead of using this approach, the position of the interface

is determined by means of test-particle computer simulations of electrons moving in the electric fields of equation (12). For electrons moving radially outward from $r=0$ with initial velocities $v_0=(2E_0/m_e)^{1/2}$ (where E_0 is the initial kinetic energy of an electron), Fig. 2 contains plots of the positions $r_{\max}$ of the electrons when they turn around, with $r_{\max}$ normalized to the position $v_0 t$ that each electron would have had if there had been no electric field. The break points in the curves occur when the turnaround distance equals the channel radius, $r_{\max}=r_{\rm ch}$, which occurs when $E_0=e^2F_{\rm casc}Y_{\rm true}/Pd_s$. For $r_{\max}\le r_{\rm ch}$ the electron behaves as a harmonic oscillator and $r_{\max}/v_0 t=2/\pi$ exactly. For $r_{\max}>r_{\rm ch}$ the curves of Fig. 2 are approximated by

$$r_{\max}/v_0 t\approx(5/2\pi)[(e^2F_{\rm casc}Y_{\rm true}/Pd_s)/E_0]^{1/2}\ .$$

Multiplying this expression by $v_0 t$ and using $v_0=(2E_0/m_e)^{1/2}$, the turnaround distance is

$$r_{\max}\approx t\frac{5}{2\pi}\left[\frac{2e^2F_{\rm casc}Y_{\rm true}}{Pd_s m_e}\right]^{1/2} \tag{14}$$

for $r>r_{\rm ch}$. Note that the initial kinetic energy of the ion E_0 has dropped out of expression (14) for $r_{\max}$. The effect of conduction-band electrons in the metal will be to shield out the electric field that is produced by the charge separation in the ion's wake. Particle-in-cell computer simulations[28] have shown that the shielding of a cylindrical charge perturbation of *arbitrarily large amplitude* in a collisionless plasma occurs in a time that is always less than $\tau_p/3$, where $\tau_p=2\pi/\omega_p$ is the plasma period. For large-amplitude perturbations the electric field is reduced with time according to $\mathcal{E}\sim\cos(2\pi t/\tau_p)$. The shielding of a time-dependent charge separation such as the one depicted in Fig. 1 will occur more slowly than $\tau_p/3$ because the conduction electrons of the metal do not begin to respond until the leading edge of the electron expansion passes over them. Additionally, the response of the conduction-band electrons could be greatly impeded by scattering off the metal lattice, since the acceleration of a conduction-band electron will substantially change its de Broglie wavelength. The electric field will be assumed to have full strength for $t<\tau_p/3$ and then it will be abruptly switched off at $t=\tau_p/3$. The interface in the electron expansion corresponds to an electron that turns around at the time when the electric field switches off (at time $t=\tau_p/3$). Thus, from expression (14), the turnaround position of the interface is

$$r_{\max}=\frac{5\tau_p}{6\pi}\left[\frac{2e^2F_{\rm casc}Y_{\rm true}}{Pd_s m_e}\right]^{1/2}\ . \tag{15}$$

Integrating the electric-field expressions (12a) and (12b) from $r=0$ to $r_{\max}$, and using expression (15) for $r_{\max}$ and expression (10) for $r_{\rm ch}$ gives the potential drop of the interface at time $\tau_p/3$:

$$\Delta\phi_{\rm trap}=\frac{eF_{\rm casc}Y_{\rm true}}{Pd_s}\left\{1+\ln\left[\frac{25}{36\pi^2}\frac{\tau_p^2F_{\rm casc}Y_{\rm true}v_0^2}{e^2z^2Pd_s}\times\left[\frac{1}{\Delta E_{\rm ch}}-\frac{1}{2m_e v_0^2}\right]^{-1}\right]\right\}. \tag{16}$$

Equations (7) and (16) form two equations for the two unknowns $Y_{\rm true}$ and $\Delta\phi_{\rm trap}$.

The pair of equations (7) and (16) are iteratively solved for $Y_{\rm true}$ and $\Delta\phi_{\rm trap}$ on a computer and the results are displayed in Figs. 3–7. In solving the equations, the electronic stopping power dE/dx of the metal target to the ion was approximated by

$$\frac{dE}{dx}=\frac{4\pi ne^4z_i^2}{m_e v_0^2}\ln\left[\frac{2m_e v_0^2}{I}\right], \tag{17}$$

where z is the charge state of the ion, v_0 is the velocity of the ion, n is the lattice density of the metal, and the subscript t is the atomic number of the metal. Expression (17) contains only the leading term in a stopping-number expansion;[29] it does not contain the relativistic correction, shell corrections, the Barkas correction, or the Block correction. The parameters taken for generating Figs. 3–7 are typical of metals, but specific to gold: the lattice density $n=5.9\times10^{22}$ cm^{-3}, the atomic number is equal to 79, the plasma period $\tau_p=4.7\times10^{-16}$ sec,[30] and the mean ionization potential $I=770$ eV.[31] The parameter Pd_s/E_* is measured to be $Pd_s/E_*\approx1.14\times10^{-9}$ cm/eV.[32,33] To evaluate Eq. (16), it is necessary to obtain a value for Pd_s from the measured value of Pd_s/E_*. This can be done by attaining a value for E_*. The quantity E_* is the average kinetic energy lost by the fast ion

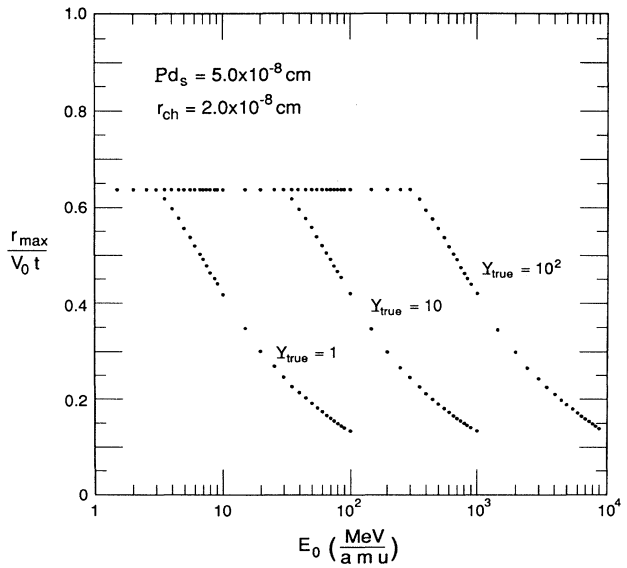

FIG. 2. Position $r_{\max}$ of an electron when it turns around (normalized to $v_0 t$) is plotted as a function of the initial kinetic energy of the electron. The points are obtained by numerically solving Eqs. (13) and (12).

per ionization produced in the target. In radiation physics, this quantity is known as the W parameter.[34] For metals, E_* has not been measured, so $E_*=25$ eV will be taken, as suggested by Sternglass,[1] which gives $Pd_s \approx 2.85\times10^{-8}$ cm. The choice of ΔE_{ch}, which determines the radius r_{ch} of the positive-charge channel, will be taken to be $\Delta E_{ch}=I/2$. Taking ΔE_{ch} larger would result in a smaller value of r_{ch}; however, a channel that is much smaller than atomic diameters will very rapidly spread owing to the orbital motions of electrons.

III. RESULTS

The numerical solutions to the pair of equations (7) and (16) are displayed in Figs. 3–7.

In Fig. 3, the trapping potential $\Delta\phi_{trap}$ [see Eq. (16)] is plotted as a function of the ion's kinetic energy per nucleon for various z values of the ion. Two trends are clearly seen: $\Delta\phi_{trap}$ increases as z increases and $\Delta\phi_{trap}$ decreases as E_0 increases. Both of these trends originate from the fact that $\Delta\phi_{trap}$ increases as the stopping power to the ion increases [see expression (17)]; i.e., more electrons are driven from the ion's wake when dE/dx is greater. For ion kinetic energies of 10 MeV/amu, potential drops of 20–900 V are predicted for fast ions from $z=1$ to 10.

The corrected secondary-electron yield Y_{true} is plotted as a function of the ion charge z for four different ion velocities in Fig. 4. The points are the results of solving expressions (7) and (16) (Y_{true}) and the solid lines are the values of the uncorrected secondary-electron yields Y_0, obtained from Eqs. (1) and (17). Note that $Y_0 \propto z^2$. Besides the trend that Y_{true} decreases as E_0 increases, two trends are seen. The first is that Y_{true} is closer to Y_0 when E_0 is larger. This indicates that the reduction in Y

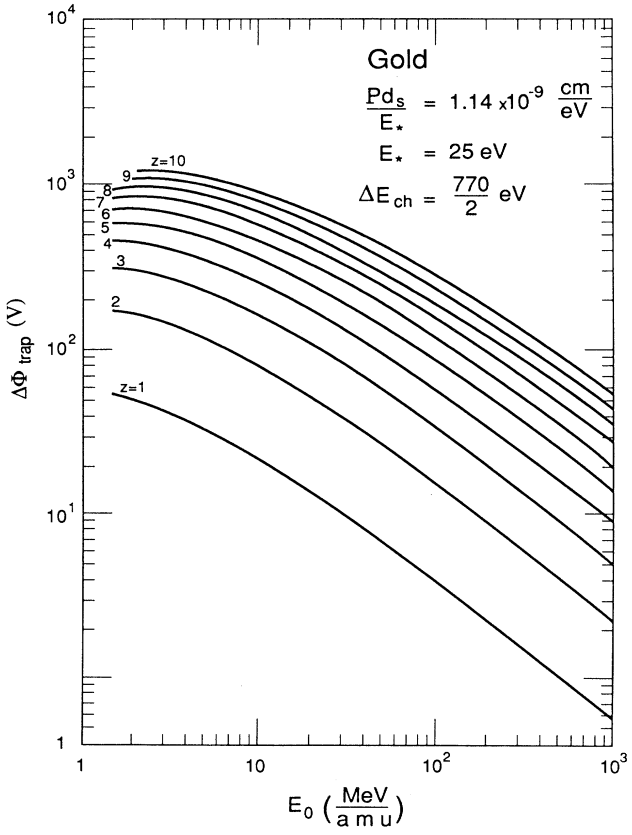

FIG. 3. Trapping potential $\Delta\phi_{trap}$ is plotted as a function of the ion kinetic energy E_0 for various z values.

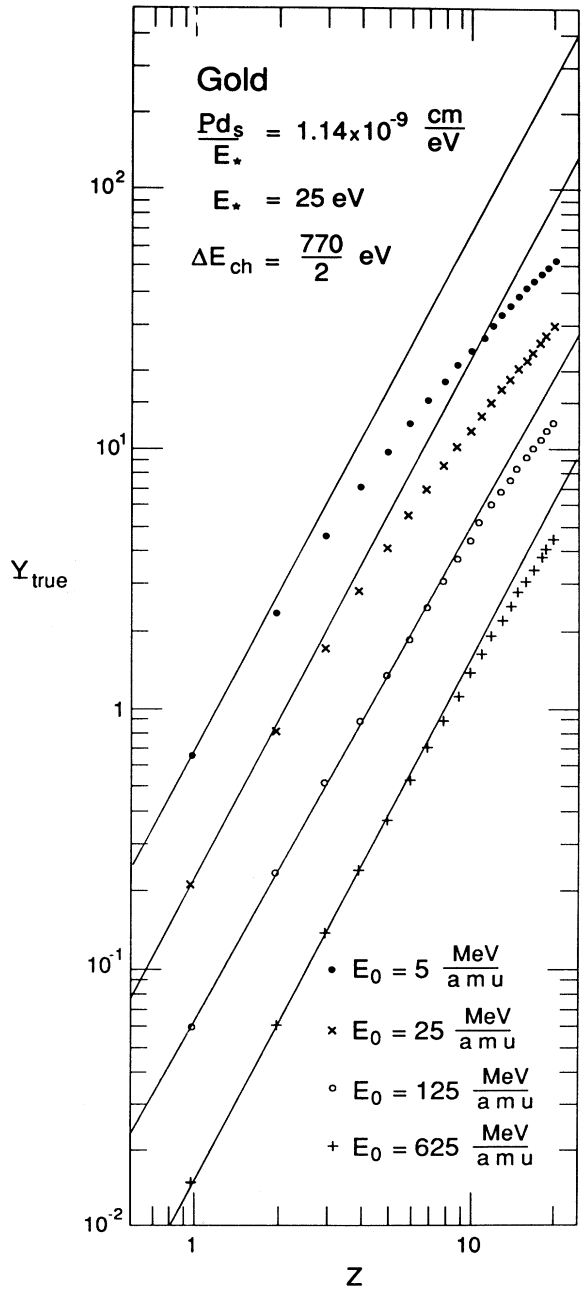

FIG. 4. Reduced secondary-electron yield Y_{true} is plotted as a function of the ionic charge z for various ion energies. The solid lines are the nonreduced yield Y_0 obtained from Eqs. (1) and (17).

owed to collective electric-field effects is less for higher-energy ions. This agrees with the trend shown in Fig. 3 that $\Delta\phi_{\text{trap}}$ decreases as E_0 increases. The second trend in Fig. 4 is that the deviation of Y_{true} from z^2 is greater as z becomes greater. Again, this is because the trapping potential $\Delta\phi_{\text{trap}}$ increases with z. The increasing deviation with increasing z has implications for the next few graphs: power-law fits of Y_{true} versus z will be made and the exponent of the fit will depend on the range of z values selected for the fit.

The effects of the choices of E_* and ΔE_{ch} on the solution Y_{true} can be seen in Fig. 5. Here, for each E_* and ΔE_{ch} value, Eqs. (7) and (16) are solved for $z=1-11$ and then a power-law fit $Y_{\text{true}}=az^s$ is performed on the 11 solutions and the resulting exponent s is plotted. The ion kinetic energy is taken to be 5 Mev/amu and $Pd_s/E_*=1.14\times10^{-9}$ cm/ev. As can be seen, the exponent s of the power-law fit is fairly insensitive to the value of ΔE_{ch} selected, so long as $0.1I\leq\Delta E_{\text{ch}}\leq I$, where $I=770$ eV is the mean ionization potential of gold. This is because the trapping potential $\Delta\phi_{\text{trap}}$ is a constant (the potential drop within the positive channel) plus a term that depends on the $\ln(r_{\max}/r_{\text{ch}})$, where ΔE_{ch} sets r_{ch} through expression (10). Hence there is only a logarithmic dependence of $\Delta\phi_{\text{trap}}$ on ΔE_{ch}. Figure 5 shows, however, that there is a strong dependence of the exponent s on the choice of E_*. By examining Eq. (16) it is seen that for Pds/E_* being fixed, $\Delta\phi_{\text{trap}}\propto E_*^{-1}$, which is a strong dependence.

The effects of the cascade process on the reduction of the secondary-electron yield can be seen in Fig. 6. Here, the exponent s of a $Y_{\text{true}}\propto E_0^s$ fit to the solutions of expressions (7) and (16) for $z=1-8$ is plotted as a function of the ion kinetic energy E_0 for three values of F_{casc}. Recall that F_{casc} is the fraction of the secondary electrons that have been ionized from the target lattice directly by two-body scattering with the ion, and that $1-F_{\text{casc}}$ is the fraction of the secondary electrons that have been ionized by other electrons. As E_0 increases, s increases toward the value $s=2$, as was seen in Fig. 4. As F_{casc} decreases, s again increases toward $s=2$. This is because when F_{casc} is small, most of the secondary electrons originate from cascade processes away from the ion's path. Hence fewer electrons are removed from the path and less of a charge separation is created. This means $\Delta\phi_{\text{trap}}$ is lower and so a smaller fraction of the electrons leaving the ion's wake are trapped.

In the final plot (Fig. 7), it is demonstrated that the reduction of the yield owed to collective electric-field effects is a strong function of the yield itself. Here, for three different ion velocities, the ratio of Y_{true}/Y_0 is plotted as a function of Y_0, where Y_{true} is the reduced secondary-electron yield and Y_0 is the secondary-electron yield predicted without accounting for collective electric

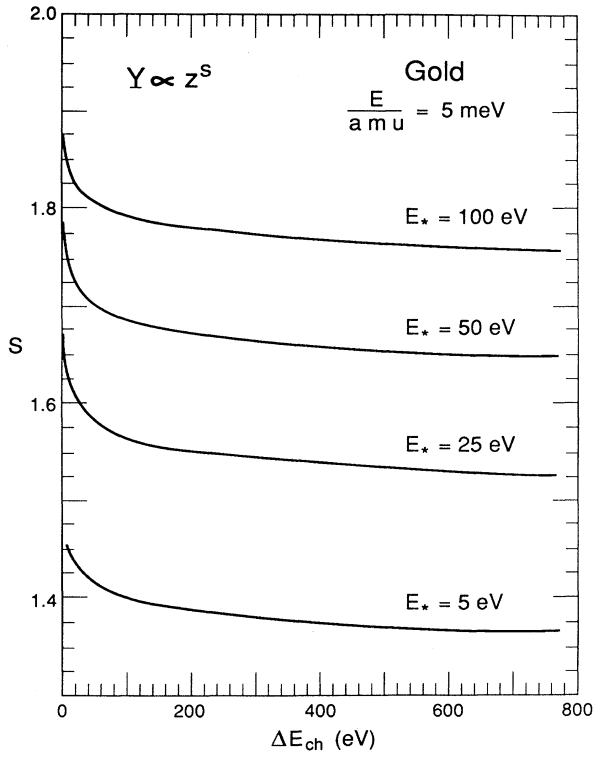

FIG. 5. Exponent s to a power-law fit of $Y_{\text{true}}\propto z^s$ is plotted as a function of the parameter ΔE_{ch} for various values of the parameter E_*.

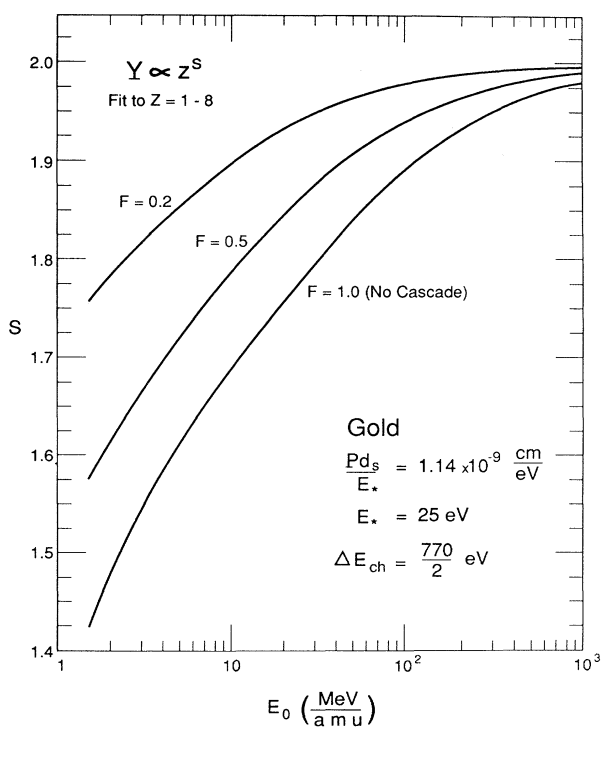

FIG. 6. Exponent s to a power-law fit of $Y_{\text{true}}\propto z^s$ is plotted as a function of the ion kinetic energy E_0 for various values of the cascade fraction F_{casc}.

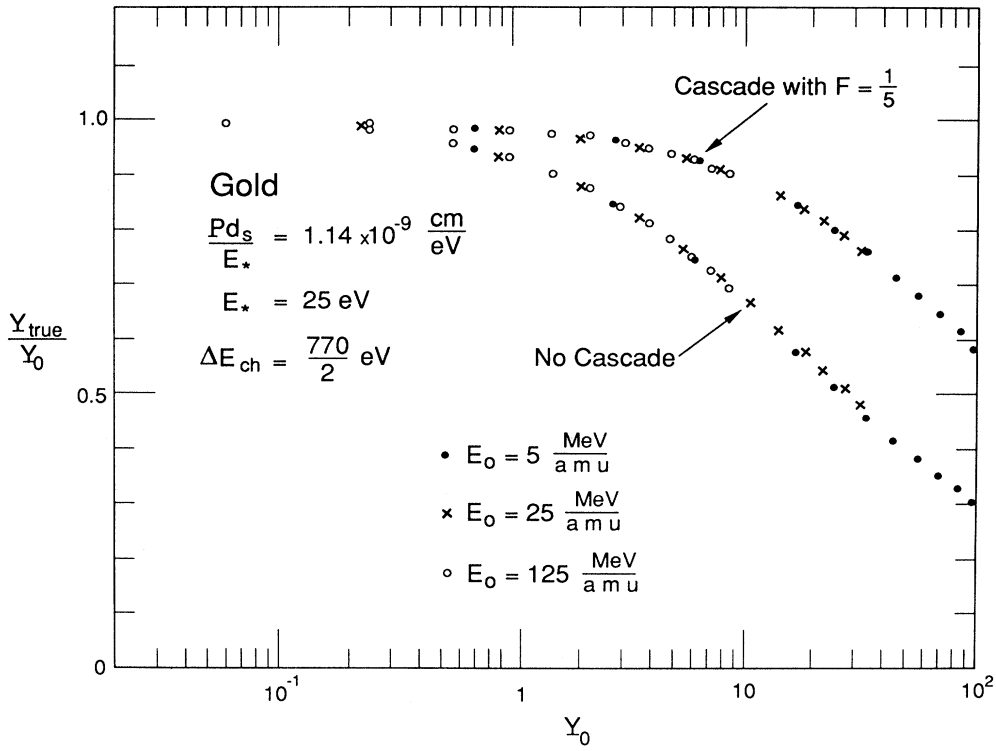

FIG. 7. Ratio Y_{true}/Y_0 of the reduced yield to the nonreduced yield is plotted as a function of the nonreduced yield for various values of the ion kinetic energy.

fields. Each point on the figure is for a different z value. For smaller yields, the reduction in the yield is slight, hence $Y_{\text{true}}/Y_0 \sim 1$; for larger yields, the reduction in the yield is great, hence $Y_{\text{true}}/Y_0 \ll 1$. This simply reflects the fact that when the yield is large, many electrons are being removed from the ion's path and so the wake electric field is strong, and thus the trapping of an electron becomes more probable. The Y_{true}/Y_0 versus Y_0 curves are seen to be nearly independent of the kinetic energy per nucleon of the ion. Although it is not shown in the figure, the curves are also nearly independent of the value of ΔE_{ch}. The curves are, however, strongly dependent on the choice of E_*.

IV. COMPARISON WITH DATA

Four sets of published data[7,8,33,35] for the yield of secondary electrons from fast, $z>1$ ions hitting metal targets will be examined in light of the results of Sec. III. Two sets will receive only a cursory examination and two will be quantitatively compared with the results of Sec. III.

The published data of Oda and Lyman[35] contain measurements of the sum of the forward and backward (entering surface and exiting surface) yields for fast ions passing through thin foils. Because the yield from the entering surface cannot be separated from the summed yield, the data will not be analyzed. The trend in the data, however, clearly indicates that the secondary-electron yield is lower than expected when the yield is large (see Fig. 6 of Ref. 35). Borovsky and Barraclough[8] measured the secondary-electron yield for 1.5–5.25 Mev/amu ^{7}Li and ^{12}C ions of various charge states hitting gold and oxidized-aluminum targets. They reported a clear trend that the secondary-electron yield was well below theoretical predictions whenever the yield was large.

Koyama *et al.*[7] published secondary-electron yield measurements for 6.2–6.5 MeV/amu He^{2+}, C^{6+}, N^{7+}, and O^{8+} ions hitting aluminum, silver, and gold targets. Fitting the $z=2$–8 data of Ref. 7 according to $Y=az^s$ obtains $s=1.72$ for aluminum, $s=1.66$ for silver, and $s=1.68$ for gold. Borovsky and Suszcynsky measured the secondary electron yield for 1.5–11 MeV/amu $^1H^{1+}$, $^3He^{2+}$, $^4He^{2+}$, $^9Be^{4+}$, $^{10}B^{5+}$, $^{12}C^{6+}$, and $^{16}O^{8+}$ ions hitting gold, oxidized-aluminum, and tantalum targets. Fitting these data according to $Y=az^s$ obtains $s=1.71$ for gold, $s=1.62$ for Al_2O_3, and $s=1.62$ for tantalum. The s values obtained for gold targets in Sec. III by modeling the wake electric field and estimating the fraction of Coulomb-scattered electrons trapped in the wake are very similar to the s values for gold obtained from the Koyama *et al.* data and the Borovsky and Suszcynsky data. Looking at Fig. 6 in the $E_0 \approx 6$-Mev/amu range, the measured value of $s=1.7$ for gold (the average of the two measured s values) corresponds to a case with $F_{\text{casc}} \approx 0.75$, i.e., cascade processes not being dominant and not being negligible in the production of secondary electrons.

V. SUGGESTED EXPERIMENTS

If higher-velocity ions are used to generate secondary electrons from metal targets, then the scaling should be closer to z^2 than the scalings are in the present experiment. According to the wake electric-field picture presented in this paper, the scaling will improve because the yield is lower for faster ions, hence the electric fields are weaker. According to Fig. 6, the exponent s of the z^s scaling relation increases monotonically with ion kinetic energy and at energies of 100 MeV/amu and higher the scaling should be nearly z^2 for $z=1-8$. To help confirm the wake model, or to eliminate some free parameters in the model, $\partial s/\partial E$ can be calculated and then compared with measurements.

Examining the energy spectra of secondary electrons produced by the various z ions can provide information about the trapping of electrons in the ion wakes. The energy spectra of Coulomb-scattered electrons in the presence of the temporally changing wake electric field can be predicted, and with the use of a cascade model (if needed) and range estimates of slow electrons in metals (e.g., Ref. 36) the spectra of electrons escaping from the metal targets can be predicted.

Experiments that would determine the values of E_* (the average kinetic energy lost per ionization produced) for metals would be of general use to calculations of the yield of secondary electrons from metal surfaces. As are the predictions of other secondary-electron models, the predictions of the wake electric-field model are sensitive to the choice of E_*. Measured values[34] of E_* for solid semiconductors, gases, and noble-gas liquids range from 3 to 50 eV.

ACKNOWLEDGMENTS

The authors wish to thank Paul Hansen for useful conversations. This work was supported by the U.S. Department of Energy Office of Arms Control.

[1]E. J. Sternglass, Phys. Rev. **108**, 1 (1957).
[2]S. N. Ghosh and S. P. Khare, Phys. Rev. **125**, 1254 (1962).
[3]P. A. Wolff, Phys. Rev. **95**, 56 (1954).
[4]J. Schou, Phys. Rev. B **22**, 2141 (1980).
[5]E. N. Sickafus, Phys. Rev. B **16**, 1436 (1977).
[6]H. A. Bethe, Phys. Rev. **59**, 940 (1941).
[7]A. Koyama, T. Shikata, H. Sakairi, and E. Yagi, Jpn. J. Appl. Phys. **21**, 1216 (1982).
[8]J. E. Borovsky and B. L. Barraclough, Nucl. Instrum. Methods Phys. Res. B **36**, 377 (1989).
[9]D. Pines and D. Bohm, Phys. Rev. **85**, 338 (1952).
[10]J. Neufeld and R. H. Ritchie, Phys. Rev. **98**, 1632 (1955).
[11]J. M. Ugalde, C. Sarasola, and P. M. Echenique, J. Phys. B **21**, L415 (1988).
[12]N. P. Kalishnikov, V. S. Remizovich, and M. I. Ryazanov, *Collisions of Fast Charged Particles in Solids* (Gordon and Breach, New York, 1985), Chap. IX.
[13]N. Rostoker and M. N. Rosenbluth, Phys. Fluids **3**, 1 (1960).
[14]I. H. Gilbert, Astrophys. J. **152**, 1043 (1968).
[15]A. J. Kalnajs, in *Gravitational N-Body Problem,* edited by M. Lecar (Reidel, Dordrecht, 1972), p. 13.
[16]P. Chenevier, J. M. Dolique, and H. Peres, J. Plasma Phys. **10**, 185 (1973).
[17]C.-L. Wang, G. Joyce, and D. R. Nicholson, J. Plasma Phys. **25**, 225 (1981).
[18]V. Decyk, *Proceedings of the 12th Conference on the Numerical Simulation of Plasmas* (Lawrence Livermore National Laboratory, Livermore, 1987), p. PM25.
[19]D. S. Gemmell, Nucl. Instrum. Methods **194**, 255 (1982).
[20]R. H. Ritchie, W. Brandt, and P. M. Echenique, Phys. Rev. B **14**, 4808 (1976).
[21]P. M. Echenique, R. H. Ritchie, and W. Brandt, Phys. Rev. B **20**, 2567 (1979).
[22]A. Faibis, R. Kaim, I. Plesser, and Vager, Nucl. Instrum. Methods **170**, 99 (1980).
[23]K. Lonngren, D. Montgomery, I. Alexeff, and W. D. Jones, Phys. Lett. **25A**, 629 (1967).
[24]D. C. Montgomery, *Theory of the Unmagnetized Plasma* (Gordon and Breach, New York, 1971), Chap. XII.
[25]X. S. Guo, Phys. Rev. A **38**, 3292 (1988).
[26]X. S. Guo, Nucl. Instrum. Methods Phys. Res. B **45**, 693 (1990).
[27]J. D. Jackson, *Classical Electrodynamics,* 2nd ed. (Wiley, New York, 1975), Sec. 13.1.
[28]J. E. Borovsky, Phys. Fluids **31**, 1074 (1988).
[29]J. Lindhard, Nucl. Instrum. Methods Phys. **132**, 1 (1976).
[30]B. R. Cooper, H. Ehrenheich, and H. R. Philipp, Phys. Rev. **138**, A494 (1965).
[31]S. P. Ahlen, Rev. Mod. Phys. **52**, 121 (1980).
[32]J. E. Borovsky, D. J. McComas, and B. L. Barraclough, Nucl. Instrum. Methods Phys. Res. B **30**, 191 (1988).
[33]J. E. Borovsky and D. M. Suszcynsky, preceding paper, Phys. Rev. A **43**, 1416 (1991).
[34]International Commission on Radiation Units and Measurements, *Average Energy Required to Produce and Ion Pair* (ICRU, Washington, D.C., 1979).
[35]N. Oda and J. T. Lyman, Radiat. Res. Suppl. **7**, 20 (1967).
[36]M. P. Seah and W. A. Dench, Surf. Interface Anal. **1**, 2 (1979).